BENNU'S CANDIDATE SAMPLE SITES AND GLOBAL SURFACE CHARACTERIZED BY SPECTRAL CLUSTERING OF OSIRIS-REX IMAGES. J. L. Rizos[1,2], J. de León[1,2], J. Licandro[1,2], D. R. Golish[3], H. Campins[4], E. Tatsumi[1,2,5], M. Popescu[6], D. N. DellaGiustina[3], M. Pajola[7], J.-Y. Li[8], K. J. Becker[9], and D. S. Lauretta[3], [1] Instituto de Astrofísica de Canarias, Tenerife, Spain (jlrizos@iac.es), [2] Universidad de La Laguna, Tenerife, Spain, [3] Lunar and Planetary Laboratory, University of Arizona, Tucson, USA, [4] University of Central Florida, Orlando, USA, [5] University of Tokyo, Tokyo, Japan, [6] Astronomical Institute of the Romanian Academy, Bucharest, Romania, [7] INAF – Astronomical Observatory of Padova, Padova, Italy, [8] Planetary Science Institute, Tucson, USA, [9] USGS Astrogeology Science Center, Flagstaff, USA.

Introduction: NASA's Origins, Spectral Interpretation, Resource Identification, and Security–Regolith Explorer (OSIRIS-REx) mission is returning a sample of carbonaceous regolith from the surface of near-Earth asteroid (101955) Bennu to Earth [1]. The OSIRIS-REx spacecraft carries a camera suite, OCAMS, consisting of three cameras: PolyCam, MapCam, and SamCam [2]. For this work, we focus on multispectral data collected by the MapCam medium-field-of-view imager, which has four passbands filters: *b′*, *v*, *w*, and *x*, with effective wavelengths at 473, 550, 698, and 847 nm, respectively. Our goal in this work is to spectrophotometrically characterize the mission's primary and backup sample collection sites, called Nightingale and Osprey, in context with the global surface of Bennu via a clustering approach. We aim to shed light on how the local-scale (candidate sample site) surface properties resemble or differ from those observed at the global scale. To fulfill our purpose, we apply the methodology described and validated in [3] to the MapCam images in a global color mosaic of Bennu and those collected at Nightingale and Osprey separately. This methodology consists of an unsupervised machine learning classification through the K-Means algorithm, which allows us to identify clusters with spectral similarities.

Data preparation: The global mosaic was built using MapCam images acquired during Flyby 2B at an altitude of 3.8 km and with a pixel scale of 25 cm [4]. For the primary and backup sample collection sites, in addition to those images acquired during the Flyby 2B, we also use higher-resolution images from Recon A at an altitude of 1.202 and 1.142 km for Nightingale and Osprey, respectively, and with a pixel scale of 6 cm. All MapCam images were calibrated to radiance factor (RADF) following the procedure described in [5]. Images were photometrically corrected using the ROLO (Robotic Lunar Observatory) photometric model by [6] to (phase, incidence, emission) = (0º, 0º, 0º) as reference angles.

Clustering analysis: We applied the K-Means algorithm [7], which is an unsupervised partitioning technique. We ran our algorithm before and after normalizing the images by dividing the reflectance value of each filter by the reflectance at 550 nm (*v* filter). To choose the optimal number of representative clusters, we employed a multiapproach criterion. We applied the Elbow method, which considers a range of number of clusters, computes the sum of squared errors (SSE) and represents this quantity against the number of clusters. The elbow position indicates a suitable number. In addition, we studied the correlation between reflectance, spectral slope, and UV behavior (*b′* filter) for each set of clusters to support the decision regarding the number of clusters.

Local-scale candidate sample sites: At both Nightingale and Osprey, we found three representative normalized clusters, of which one (red) is concentrated in the darkest areas, showing an inverse correlation between reflectance and spectral slope, and also between *b′* normalized reflectance and slope. The red cluster in Nightingale (**Figure 1**) presents the reddest spectra observed overall, $(-0.3\pm1.0) \times 10^{-3}$ %/1000 Å. For Nightingale, the clusters shown in red and blue allow us to measure UV upturn or absorption band at 550 nm, whereas the cluster shown in green presents a possible absorption feature at 700 nm.

At Osprey (**Figure 2**), again the red and blue clusters emphasize the UV upturn, but also the three clusters show a small upturn in the *x* filter, making it possible to measure a shallow absorption at 700 nm.

We are not able to identify a clear absorption band either at 550 or 700 nm when we impose a 3σ criterion; however, we find possible hints of absorptions.

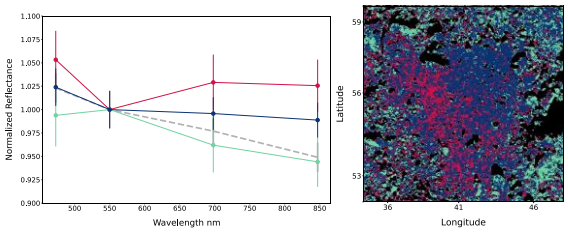

Figure 1. Results from the application of the clustering technique to the normalized Recon A images of Nightingale. For comparison, we include a dashed gray line to show the average normalized Bennu spectrum. On the left, the three representative spectral clusters with the corresponding error bars (standard deviation) are labeled with different colors. On the right, the location of the identified clusters over the analyzed area, using the same color code. Black pixels are those that are out of the defined limits: DN > 14000, RADF < 0.027, emission or incidence angles > 80º).

Both Nightingale and Osprey have spectra redder than 1σ from average. Based on the crater chronology by [4], this suggests that their craters could have been formed within the past 100,000 years. The red-cluster material outside the crater at Nightingale (see left lower area in **Figure 1** or upper yellow circle in **Figure 3**) could be an ejecta ray from its crater, indicating recent formation. Such a morphology can be seen for the artificial crater on asteroid (162173) Ryugu created by the Hayabusa2 mission [8]. The lack of an ejecta ray at Osprey is consistent with an older crater formation age than Nightingale.

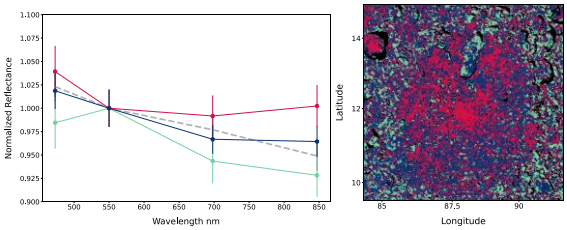

Figure 2. Same as **Figure 1**, but for Osprey.

Global mosaic: The global surface of Bennu is characterized by four clusters scattered across the surface. They indicate heterogeneity in terms of albedo, corresponding with the bright and dark boulder groups identified in [4], where this reflectance dichotomy is attributed to primordial heterogeneity. The lowest- and highest-albedo clusters in this study are distributed on rockier terrains. The intermediate-albedo clusters might be the regolith mixture of those two components (**Figure 3**). Once we normalize the images, our analysis identifies three clusters, also associated with boulders of different reflectance, in which the main difference is in spectral slope and UV value. We find a cluster occupying ~50% of the surface showing spectral behavior in agreement with the ground-based Bennu spectra (blue) [9]. The rest of the surface is divided into two clusters: one covering 21% of the surface and presenting both the lowest near UV value and the lowest spectral slope, $(-2.0 \pm 0.5) \times 10^{-3}$ %/1000 Å (green); and one covering 26.6% of the surface and presenting a near UV-upturn (or a drop at 550 nm) and the most positive spectral slope, $(-1.6 \pm 0.5) \times 10^{-3}$ %/1000 Å (red). The red cluster corresponds to darker boulders and small craters, whereas the green one corresponds to the brightest areas distributed over the surface. Both Nightingale and Osprey, which are inside of craters, are classified into red clusters within this global analysis, suggesting being composed by fresher material.

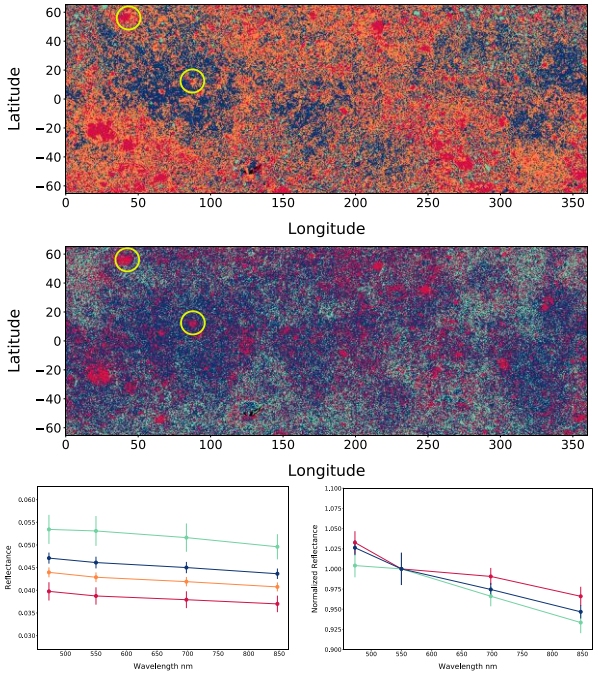

Figure 3. Same as **Figure 1**, but for the global mosaic of Bennu. On top is shown the analysis in absolute reflectance, whereas the middle is after normalizing the images. Yellow circles mark Nightingale and Osprey. The spectra are shown on the bottom, unnormalized on the left, normalized on the right.

Acknowledgments: We thank the entire OSIRIS-REx Team for making this mission possible. This research has made use of the USGS Integrated Software for Imagers and Spectrometers (ISIS3). OCAMS/MapCam images collected during Detailed Survey and Recon A are available via the Planetary Data System [10]. This material is based upon work supported by NASA under Contract NNM10AA11C issued through the New Frontiers Program.

References: [1] Lauretta et al. (2017) Space Sci. Rev. 212, 925–984. [2] Rizk et al. (2018) Space Sci. Rev. 214, 26. [3] Rizos et al. (2019) Icarus 328, 69–81. [4] DellaGiustina et al. (2020) Science 370, eabc3660. [5] Golish et al. (2020) Space Sci. Rev. 216, 12. [6] Golish et al. (2020) Icarus 113724. [7] MacQueen (1967) Proc. Fifth Berkeley Symp. Math. Stat. Probab. 1, 281–297. [8] Arakawa et al. (2020) Science 368, 67–71. [9] Clark et al. (2011) Icarus 216, 462–475. [10] Rizk et al. (2019) urn:nasa:pds:orex.ocams.